Noname manuscript No.

An Electrochemiluminescence Biosensor based on Graphitic Carbon Nitride Luminescence quenching for Detection of AFB_1

Dongyan Tian[1], Chao Lv[1], Haihan Zou[1], Jie Wang[1], Qiandong Zhuang[2], Songmei Wu[1], Yu Yu[1,*], Kejian Ding[1,*]

[1] School of Science, Beijing Jiaotong University, Beijing 100044, P.R. China.

[2] Physics Department, Lancaster University, Lancaster, LA1 4YB, UK.

Corresponding Author E-mail: dkjian@bjtu.edu.cn; yuyu@bjtu.edu.cn

Acknowledgments

This work was supported by National Key Research and Development Plan of China (2017YFC0805900), the National Natural Science Foundation of China (NSFC 51972017, 21503013), the Fundamental Research Funds for the Central Universities of China (2019JBM409, 2019JBM326).

*Corresponding Author: Kejian Ding; Yu Yu
School of Science, Beijing Jiaotong University, Beijing 100044, P.R. China.
Telephone: +86-010-51684352.
E-mail: dkjian@bjtu.edu.cn; yuyu@bjtu.edu.cn

Abstract Based on graphitic carbon nitride (g-CN) nanocomposites coupled with aptamer, a regenerable electrochemiluminescence (ECL) biosensor is developed for the quantitative detection of aflatoxin B_1 (AFB_1) In the presence of AFB1. In the existence of AFB_1, the structure of the aptamer changed into a loop, and the original ECL signal was decreased due to the enhancement of luminescence quenching between the ferrocene attached to the end of the aptamer and the luminescent substrate g-CN. Moreover, AFB_1 with oxidation state could also react with high energy state g-CN, leading to further reduction of the electrochemiluminescence signal. Under the optimal conditions, the ECL intensity decreased linearly on the AFB_1 concentration in the range of 0.005 to 10 ng/mL, with a detection limit of 0.0037 ng/mL. We have also demonstrated that the g-CN based biosensor was selective for AFB_1 and performed on rice samples, which demonstrate a prospective application in non-enzymatic AFB_1 detection.

Keywords Electrochemiluminesce aptasensor · Aflatoxin B_1 · Graphitic carbon nitride · Luminescence quenching

1 Introduction

Aflatoxins are a class of carcinogenic mycotoxins produced by Aspergillus fungi, and aflatoxin B_1 (AFB_1) is the most carcinogenic substance among them. Previous studies have shown that AFB_1 can cause hepatocellular carcinoma as well as malnutrition, growth impairment, and immune disorders[1]. Aspergillus flavus pollutes many crops including peanut, corn, and rice as it widely exists in the soil, which will potentially

cause a lot of cost to remove the toxin produced by it[2]. On account of the harmfulness and universality of AFB_1, there is a huge demand to establish a rapid, effective, and highly sensitive analytical method to trace the presence and the amount of AFB_1 in crops and food, which is essentially important for toxicity assessment, post-harvesting processing, food safety and environmental monitoring.

At present, the commonly used AFB_1 detection methods mainly include thin layer chromatography (TLC), liquid chromatography (LC), gas chromatography (GC), liquid chromatography-mass spectrometry (LC-MS/MS), and immunochemistry[3-5]. Despite safety and sensitivity of these chromatography methods, they suffer from several major drawbacks including expensive instruments, complex pretreatment, and trained persons. Though immunochemistry has porotential to simplify processing procedures, the antibodies involved encounter limitations in stability and cost. Therefore, new detection methods are urgently being explored.

The exploration of new methods for the detection of trace AFB_1 has facilitated the development of Photoluminescence (PL) , chemiluminescence (CL) and electrochemiluminescence (ECL) [6]. Amongst these technologies, the ECL has been proposed to be the most promising method owing to several advantages, e.g. improved reproducibility due to its capability of controlling the luminescence reaction time and position, no background signal and high sensitivity, and linear dependence over a wide range of AFB1 concentration [7]. The AFB_1 trace detection method based on ECL is highly valuable.

Using graphitic carbon nitride (g-CN) as a new kind of ECL emitter has many strengths

such as large surface area with good stability for its triazine ring structure, excellent photochemical properties, and low-cost synthesis procedure[8]. Furthermore, g-CN can be modified readily with nanomaterials such as carbon dots[9], Au nano-paticles[10], and aptamers[11] for various biosensing applications.

A good ECL sensor requires not only an ECL emitter, but also a corresponding identification unit. In recent years, with the discovery and application of aptamers, antibodies are no longer unique in molecular recognition by different biosensor detection techniques[12]. Aptamers have many potential advantages over traditional antibodies, such as high specificity, minimized inter-batch variation, and reduced side effects[13]. These advantages have attracted much research attention as a powerful tool for molecular recognition. The aptamers have been successfully applied in detection of heavy metal ions[14], proteins[15], and molecules[16].

Moreover, the combination of the ECL emitter and the identification unit will affect the luminous efficiency and stability of the ECL sensing composite material. For example, modifications taking weak intermolecular force to link aptamer and g-CN like π-π stacking interactions[11] could be influenced by temperature and ionic strength. Therefore, it is necessary to combine g-CN with nanomaterials through covalent bonds with more stable structure for efficient photochemical signal output and shortening of electronic transmission distance such as amide bond.

Using DNANT-based signal amplification[17] and ratiometric aptasensor[18], ECL aptamer sensors have demonstrated improved performance in AFB_1 detection such as enhanced specificity and increased sensitivity in comparison with traditional methods .

Commented [ZQ1]: Defined before?

However, practical application requires a technology that is convenient and more effective without complex and unstable ECL aptamers with multi-step. Herein, we propose a more stable and simpler AFB_1 electroluminescence sensing platform based on g-CN junction aptamers, with enhanced specificity, increased detection limit and imporoved sensitivity. For aptamer with the same host sequence, different chain lengths have a large impact on detection specificity[19]. Therefore, after comparison, we selected the most suitable length of aptamer to achieve specific sensitive detection of AFB_1. In order to obtain a more stable and reproducible aptamer sensor, we used an amidation reaction to link the aptamer to g-CN. BSA was used as blocking agent to reduce non-specific adsorption. In the presence of AFB_1, aptamers modified on the g-CN surface selectively binds to AFB_1, and energy transfer and electron transfer occur between g-CN and the ferrocene attached to the end of the aptamer. The indentation of the spatial distance enhances the quenching effect and reduces the ECL signal, as shown in Scheme 1(b). Here, ferrocene was used as a quencher to quench high energy g-CN. By detecting the different attenuation degrees of the ECL signal of the sensor, the high-sensitivity determination of trace detection AFB_1 was realized. Furthermore, the ECL biosensor was used to detect AFB_1 for rice samples which produced satisfied results. and satisfactory results were obtained.

Commented [ZQ2]: Here should give a value or a justification to convince readers the how results are satisfied.

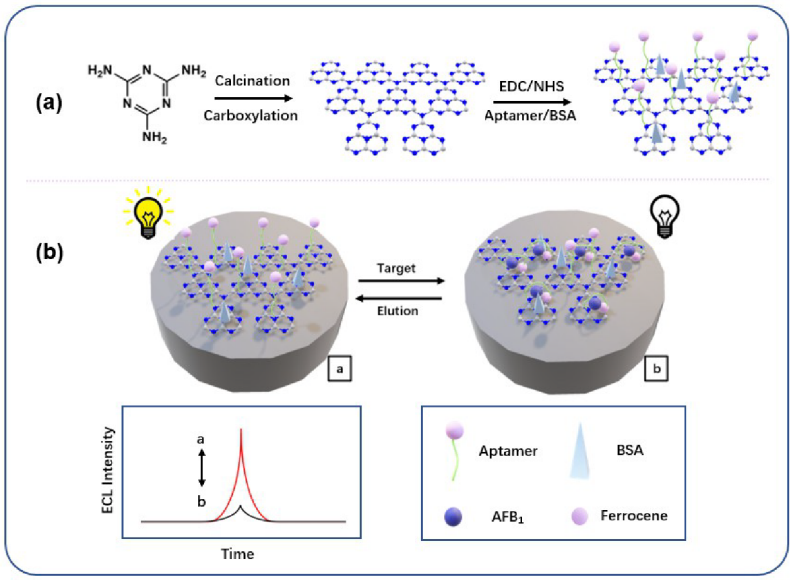

Scheme 1 (a) Composite material fabrication process. **(b)** Detection mechanism of ECL biosensor.

2 Experimental sections

2.1 Reagents and materials

The following part displayed the aptamer nucleotide sequence: 5′-NH_2-C_6-CGTGTTGTCTCTCTGTGTCTCG-Fc-3′ (APT), which had been synthesized and purchased from Sangon Biotechnology Co. Ltd. (Shanghai, China). Urea and 1-hydroxypyrrolidine-2,5-dione (NHS) were purchased from Sinopharm Chemical Reagent Co., Ltd. Nitric acid was purchased from Beijing Chemical Works. Ethanol come from Tianjin Fuyu Fine Chemical Co.,Ltd. 1-(3-Dimethylaminopropyl)-3-ethylcarbodiimide hydrochloride (EDC), Bovine Serum Albumin (BSA), Aflatoxin B_1 (AFB_1), and Ochratoxin A (OTA) were obtained from InnoChem. Sodium persulfate ($Na_2S_2O_8$) was purchased from Acros organics (Janpan). Phosphate buffer solutions (PBS) of pH = 7.4

was prepared using PBS tablets from Solarbio (Beijing, China) containing 0.1 M KCl as a supporting electrolyte. All reagents were analytical grade or better, and all chemicals were used directly without further purification. Pure water (15 MΩ) used in the experiments was supplied by a Millipore System (Milli Q).

2.2 Apparatus

The MPI-E electrochemiluminescence analysis system from Xi'an Remex Analysis Instrument Co.,Ltd. (China) (http://www.chinaremex.com) was used to perform the ECL detection. A VersaSTAT 3 electrochemical workstation from Ametek Scientific Instrument (USA) (https://www.ameteksi.com/) was used for cyclic voltammetry (CV) and electrochemical impedance spectroscopy (EIS) detection, with a three-electrode system, the working electrode was glassy carbon electrode (GCE, Φ = 4 mm), a platinum grid was taken as counter electrode, and Ag/AgCl (sat. KCl) was carried as the reference electrode, respectively. The spectrum was measured using a SPECTRUM 400 FTIR system using the KBr disk method. The crystalline structure was investigated by transmission electron microscopy (TEM) at 200 kV (JEOL-2100F). Atomic force microscopy (AFM) images was acquired through tapping-mode (Nanosurf).

2.3 Synthesis of Materials

2.3.1 Synthesis of carboxylated g-CN

The bulk g-CN was synthesized following a classical route with some modifications[20]. 30 g of urea was evenly placed in an alumina crucible, then covered

with the same alumina crucible, heated to 550 ℃ in a muffle furnace at a heating rate of about 10 ℃/min and maintained at the same temperature for 4 h. After naturally cooling to room temperature, the resulting pale-yellow powders were ground in an agate mortar. In order to obtain smaller powders, the milled product was sieved into subsieve size. Product generation rate was about 4%. After soaking and ultrasonicating for 2 h with dilute nitric acid, the mixture was centrifuged at 9000 rpm. 1 g of g-CN precipitate and 100 mL of HNO_3 (5 M) were refluxed for 24 h at 125 ℃ and cooled down to room temperature naturally. After that, the mixture was centrifuged at 12000 rpm and washed thoroughly with deionized water several times until the pH reached neutral. At last, the acquired product was dried in the vacuum oven for 12 h at 35 ℃ to obtain the carboxylated g-CN.

2.3.2 Preparation of g-CN-APT

1 mg carboxylated g-CN was dissolved in 0.01 M PBS solution for further use. 2 mL of the mixture was activated by 1 mL of 40 mM EDC and 10 mM NHS, which was stirred for 0.5 h. Afterwards, 1 mL of APT (0.4 μM) was added into above mixture and incubated for 1 h at 4 ℃ for further use.

2.4 Electrode modification and ECL sensor fabrication

firstly, 1.0, 0.1, and 0.05 μm alumina slurry were sequentially utilized to polish GCE, followed by sonicating in ethanol and ultrapure water for 60 s, respectively. It was then dried under infrared lamp irradiation. Secondly, 5 μL of the g-CN-APT was dropped

onto the electrode and dried under nitrogen gas. Thereafter, the aptasensor was immersed in a 0.1% BSA solution for 1 h in order to block the non-specific site. The electrode was washed by 0.01 M PBS for three times and dried under nitrogen gas. As a result, ECL biosensor (g-CN-APT/BSA/GCE) was obtained and stored at 4 C°.

2.5 ECL measurements

2.5 μL of different concentrations of AFB_1 solution were dropped on the modified electrode and incubated for 15 min. The three-electrode system was inserted into PBS (0.1 M, pH=7.4) containing 100 mM $Na_2S_2O_8$ and 100 mM KCl in an ECL detector cell for the ECL detection. The cyclic voltammetry scan was from 0 to -1.6 V at a scan rate of 0.1 V/s and the voltage of photomultiplier tube (PMT) was set at 600 V. The average values of ECL intensity peaks for multiple cycles were recorded for quantitative analysis. The error bars showed the standard deviation of the three times measurements. All ECL measurements were taken at room temperature.

2.6 Sample analysis

Fresh rice sample purchased from the local market was ground in the laboratory. First of all, 5 g of the sample was added in 20 mL of ethanol-water (1:1 v/v). it was then sonicated for 30 min followed by centrifuging at room temperature to extract the sample. The supernatant was diluted with ultrapure water, which was then used as blank sample. The spiked samples with various concentrations of AFB_1 were used as analytical samples. Each sample was measured three times to obtain the AFB1 concentration.

3 Results and discussion

3.1 Characterization of g-CN

The XRD of g-CN (Fig. S1(a)) exhibits two characteristic peaks centered at 13° and 27°, which are related to the (100) plane and the (002) plane of g-CN respectively. This preliminary result indicates the stacking of aromatic structures and confirms the succsefful fabrication of g-CN [21]. Pure g-CN was peeled from the large fragments. As shown in Fig. 1(a) and Fig. 1(c), TEM and AFM images are featured with lamellar morphology and planar thickness, which revealed the thin graphitic-like structure of the g-CN materials [22]. The average layer thickness was about 5.1 nm. On the basis of these results, it was proved that g-CN with few layers had been synthesized successfully. The structure of the prepared carboxylated g-CN was also characterized by TEM as shown in Fig. 1(b). It illustrates a thinner and more fragmented structure with more defects compared with g-CN, which is attributed to the subsequent amidation to g-CN. FTIR spectroscopy (Fig. S2) indicates that carboxylated g-CN retained all the typical bands of g-CN. The strong absorption band at 810 cm^{-1} was referred to the bending vibration of triazine ring and heptazine ring units. For the carboxyl group associated with hydrogen bonding, the O-H has a broad and scattered stretching vibration absorption peak in the range of 2500 to 3300 cm^{-1}. The absorption peak at 1405 cm^{-1}, 1459 cm^{-1}, 1573 cm^{-1}, and 1639 cm^{-1} was derived from the stretching vibration of the heptazine ring[22]. Compared with g-CN, the extra absorption bands at 1334 cm^{-1} and 1430 cm^{-1} come from the stretching vibration of the nitro group. The absorption peak

at 1720 cm^{-1} is likley correspond to the bending band of C=O[6]. Fig. S3 (a and b?) shows the UV-Vis absorption spectra of g-CN and carboxylated g-CN, respectively. The results illustrate that the maximum absorption peak of g-CN is 320nm, while the maximum absorption peak of carboxylated g-CN is 313nm. this indicates that carboxylated g-CN has smaller particle size, thinner layer and larger band gap compare with g-CN, which will facilitate further modification of the luminescent substrate.

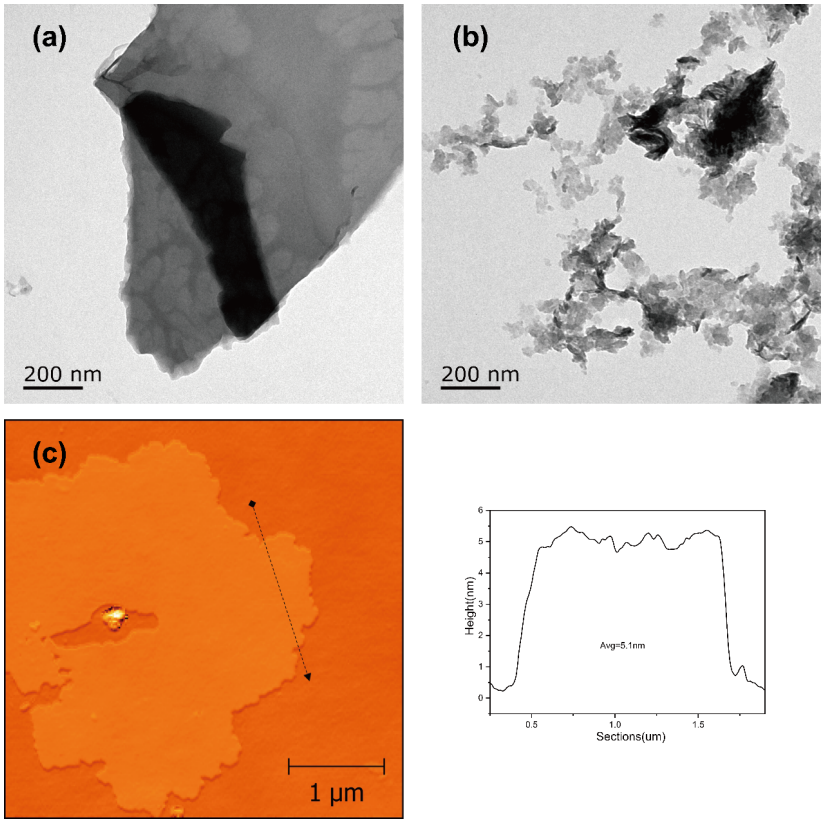

Fig. 1 TEM image of **(a)** g-CN and **(b)** carboxylated g-CN **C** AFM image of g-CN

3.2 The possible ECL mechanism

The operation principle of the fabricated biosensor is revealed in Scheme 1(b). As a coreactant, $S_2O_8^{2-}$ greatly improve the luminous efficiency of g-CN, which can be demonstrated in the Fig. S4(a). The presence of the specific aptamer APT makes the luminescent substrate g-CN selective for AFB_1 as shown in the Fig. S4(b). When the target AFB_1 is present in the system, the aptamer will spatially fold and surround the AFB_1. The ferrocene at the free end of the aptamer will be close to the substrate g-CN, thereby enhances the quenching effect which results reduced ECL signal. Meanwhile, is as a powerful oxidant, $S_2O_8^{2-}$ may oxidize AFB_1 to AFB_1 oxidation products[23]. During the quenching process, there may be a case where the energy of high energy state g-CN (g-CN^*) is transferred to the AFB_1 oxidation product, resulting in a further decrease in ECL intensity. However, as a result of AFB_1 cannot exist in the reaction cell for too long, we could only measure for the beginning period of time. Moreover, the reduced ECL signal was directly related to the concentration of AFB_1. Thus, we established the relationship between ECL signal attenuation and AFB_1 concentration. The specific reaction process is shown in the equations[24].

Without AFB_1:

$$\text{g-CN}+e^- \rightarrow \text{g-CN}^{\cdot-} \quad (1)$$

$$S_2O_8^{2-}+e^- \rightarrow SO_4^{2-}+SO_4^{\cdot-} \quad (2)$$

$$\text{g-CN}^{\cdot-}+SO_4^{\cdot-} \rightarrow \text{g-CN}^*+SO_4^{2-} \quad (3)$$

$$\text{g-CN}^* \rightarrow \text{g-CN}+hv \quad (4)$$

With AFB_1:

$$g\text{-}CN^{*}+Fc \rightarrow g\text{-}CN+Fc^{*} \quad (5)$$

And

$$S_2O_8^{2-}+AFB_1 \rightarrow SO_4^{2-}+AFB_{1_{OX}} \quad (6)$$

$$g\text{-}CN^{*}+AFB_{1_{OX}} \rightarrow g\text{-}CN^{+}+AFB_{1_{RE}} \quad (7)$$

3.3 Biosensor characterization and detection feasibility assay

ECL was used to detect the preparation of modified electrodes. Electrochemical luminescence was continuously scanned in a range of 0 to -1.6 V in 0.1 M PBS (0.1 M $Na_2S_2O_8$) at a rate of 100 mV/s. The Fig. 2(a) gives a plot of the time versus the corresponding luminescence signal intensity. It can be seen that the luminescence peak value of the electrode loaded g-CN-APT (Fig. 2(a), curve b) increases sharply compared to the bare electrode (Fig. 2(a), curve a), which is due to the integrity of redox system. The g-CN-APT is introduced to GCE surface to make the luminescence system intact, showing that the sensor material has been successfully modified on the electrode surface. When BSA is assembled to the nanocomposite, BSA will slow the transmission of electrons, resulting in a decrease in luminescence intensity (Fig. 2(a), curve c). After the introduction of AFB_1, the luminescence intensity sharply decreases (Fig. 2(a), curve d), which indicates that the quenching effect has occurred on the electrode surface, and the detection purpose was achieved. in addition, the luminescence intensity was found to be recovered (Fig. 2(a), curve e) after the modified electrode was washed in 0.1 M KOH, suggesting that the AFB_1 had been removed from the electrode surface, e.g. a successful regeneration of the sensor.

We also used electrochemical impedance spectroscopy (EIS) to study the surface characteristics of the modified electrode in $[Fe(CN)_6]^{3-}/[Fe(CN)_6]^{4-}$ (10 mM) solution containing KCl (0.1 M). Fig. 2 shows the EIS curve of the electrode modification process and corresponding impedance spectrum changes. The bare GCE gives a small semicircle (Fig. 2(b), curve a), which means the charge transfer resistance is small. Compared to bare GCE, the semiconducting properties of g-CN may slow the transfer rate of electrons on the surface of GCE, and the negatively charged aptamer and $[Fe(CN)_6]^{3-/4-}$ have electrostatic repulsion, thus significantly increases the charge transfer resistance (Fig. 2(b), curve b). We used BSA to occupy the exposed position of biosensor so as to eliminate non-specific adsorption, which also led to impeded electron transfer (Fig. 2(b), curve c). A decrease would appear in the charge transfer resistance after the nucleic acid aptamer captured AFB_1 (Fig. 2(b), curve d). These results clearly demonstrate the successful manufacture of the ECL biosensor.

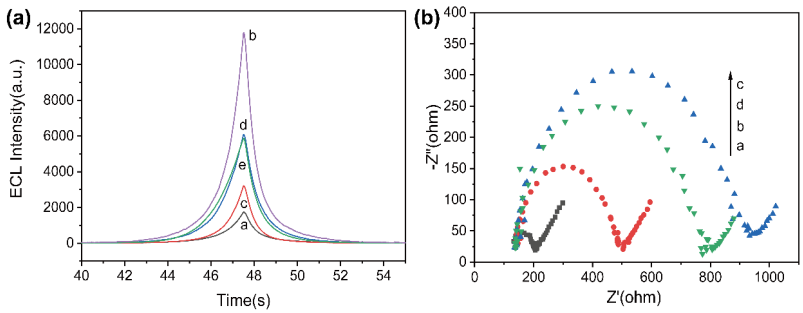

Fig. 1 (a) ECL intensity profiles of different modified electrodes: **a** bare GCE, **b** GCE/g-CN-APT, **c** GCE/g-CN-APT/BSA/AFB_1, **d** GCE/g-CN-APT/BSA, and **e** GCE/g-CN-APT/BSA after the first regeneration measured in PBS (pH = 7.32)

containing 0.1 M KCl and 0.1 M $S_2O_8^{2-}$. **(b)** Electrochemical impedance spectroscopy (EIS) behaviors of different modified electrodes: **a** bare GCE, **b** GCE/g-CN-APT, **c** GCE/g-CN-APT/BSA, and d GCE/g-CN-APT/BSA/AFB_1. Experimental conditions of EIS: 10 mM $K_3Fe(CN)_6/K_4Fe(CN)_6$ (1:1) with 0.1 M KCl solution.

3.4 Optimization of experimental conditions

To achieve a highly sensitive detection, we optimized several importatn experimental parameters including g-CN preparation temperature, $S_2O_8^{2-}$concentration, pH, and ionic strength.

As shown in Fig. 3(a), with increase of the g-CN preparation temperature , the electrochemical luminescence intensity increases and reaches a maximum at 570 ℃,then decreases with further increasing. This is because the particles prepared at higher temperatures have a smaller particle size, higher luminous efficiency, and larger band gap[25]. However, an excessively large band gap may also make the luminescence wavelength shorter than the detection range of the instrument. Moreover, the g-CN luminescence intensity prepared at 550 ℃ is similar to the one prepared at 570 ℃, but the yield is higher, so we choose 550 ℃ as the best g-CN preparation temperature. When the $S_2O_8^{2-}$ concentration is 0.1 M, the ECL luminescence intensity is maximal (Fig. 3(b)). As the $S_2O_8^{2-}$ concentration increases, the ECL intensity gradually increases, and then ECL signal has no longer any obvious change at 0.1 M, which indicates that co-reactant is sufficient at this time. So the 0.1 M concentration was chosen for subsequent experiments. From Fig. 3(c), as the pH increases from 5.6 to 9.0, the luminescence capacity of the ECL sensing system first increased and then diminished,

which was caused by the weakening of the luminescence quenching effect of AFB_1 decomposition by the high pH environment. Therefore, the optimal pH is close to 7.4 for the entire experiment. Subsequently, the effect of ionic strength on luminescence quenching was examined (Fig. 3(d)). KCl provides conductivity and affects ECL light-emitting systems at low ionic strength; it is found that the luminescence ability of the ECL system is independent to the high ionic strength.

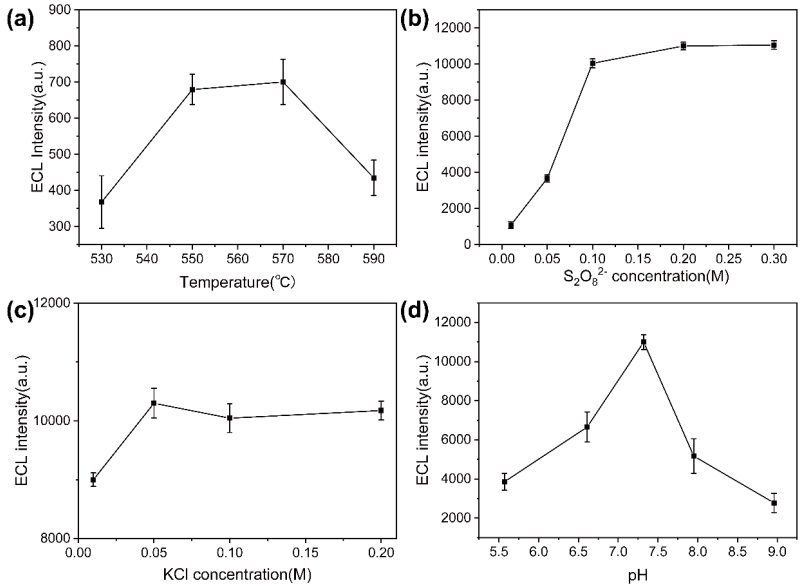

Fig. 2 Effect of **(a)** preparation temperature of g-CN on the response of ECL intensity from GCE/g-CN with voltage of PMT was 300 V, **(b)** concentration of $S_2O_8^{2-}$ on the response of ECL intensity from GCE/g-CN with voltage of PMT was 600 V; **(c)** the effect of ionic strength, and **(d)** pH value.

3.5 Calibration plot and detection limit

After determining the optimal conditions, the sensor performance was evaluated by measuring the ECL intensity at a range of different AFB_1 concentrations. It can be seen from Fig. 4(a) that the ECL intensity gradually decreases with the AFB_1 concentration increases. The reason for this phenomenon is that the aptamer binds to the target AFB_1, and the high-energy state g-CN and the Fc on the aptamer end reduce the ECL signal intensity through energy transfer and photoexcitation electrons. In addition, the ECL intensity changes linearly with the logarithm value of AFB_1 concentration. Fig. 4(b) shows the sensor's determination of AFB_1 standard curve. The linear regression equation could be expressed as I = -555.65logc(ng/mL) + 3917. The linear range of the determination is 0.005ng/mL to 10ng/mL, the correlation coefficient R^2 = 0.9906, and the detection limit is calculated to be 0.0037ng/mL (3σ). Compared with previous reports on AFB_1 measurements (as shown in Table 1), the sensor has a relatively low detection limit and a wide linear range.

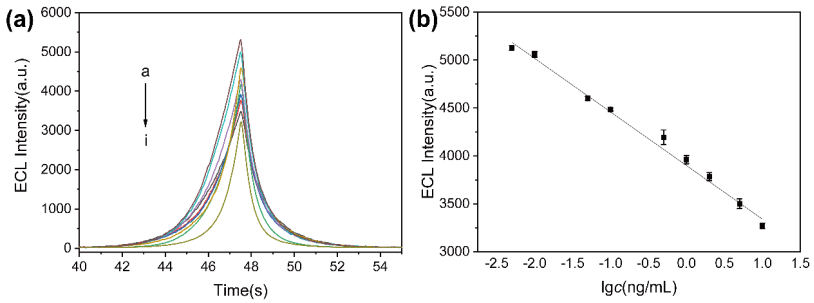

Fig. 3 (a) The corresponding ECL behaviors of the biosensor to AFB_1 with the concentration: **a** 0.005 ng/mL, **b** 0.01 ng/mL, **c** 0.05 ng/mL, **d** 0.1 ng/mL, **e** 0.5 ng/mL,

f 1 ng/mL, **g** 2 ng/mL, **h** 5 ng/mL, and **i** 10 ng/mL. **(b)** The calibration plot for AFB_1.

Table 1 In contrast to other previously reported AFB_1 biosensors

Analytical method	Linear range	Limit of detection	Reference
Fluorescence	0.03-0.9 ng/mL	0.008 ng/mL	[26]
DPV	0.05-6.0 ng/mL	0.05 ng/mL	[27]
ECL with ELISA	0.1-100 ng/mL	0.033 ng/mL	[28]
Electrochemical	0.005-50 ng/mL	0.0045 ng/mL	[29]
ECL	0.005-10ng/mL	0.0037ng/mL	This work

3.6 Stability and selectivity

In order to test the stability of the constructed sensor, we performed several cycles of continuous scanning of the cultured electrode (Fig. 5), and it showed satisfactory results. In order to verify its reproducibility, the modified electrode was washed and regenerated several times, and it was found that its adaptability did not change within a certain number of times (Fig. S5).

Commented [ZQ3]: Better to show what is the variation (there must be) with uncertainty of the measurements.

Commented [ZQ4]: How many times?

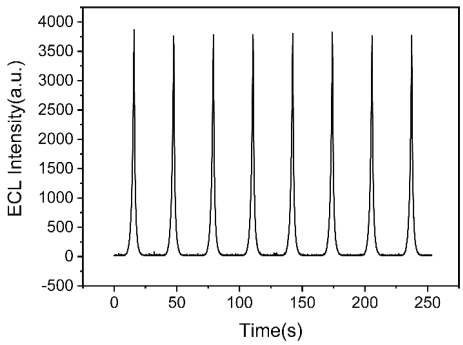

Fig. 4 The stability of the proposed biosensor with 2ng/mL AFB_1.

We also evaluated the response of the designed biosensor to other small molecule interfering substances (Fig. S6). The disturbance detection of OTA as a sensor was studied. We found that the change of the ECL intensity of the sensor is negligible compared to the blank. However, when a mixture of AFB_1 and OTA was used as the detection object, the ECL intensity of the sensor did not change significantly compared to the case of sole AFB_1. The above results show that the sensor possesses good selectivity. However, this work cannot detect two or more kinds of small molecules at the same time, which may limit its application.

3.7 Real samples analysis

Commented [ZQ5]: Real-time analysis?

In order to verify the applicability of the developed sensor in actual sample analysis, different concentrations of AFB_1 were incorporated into rice samples for recovery experiments. As shown in Table S1, recovery values (from 96.2% to 103.1%) indicate that the interference from complex sample matrices has little effect on detection. The slight effect of OTA may be due to non-specific adsorption. The results show that the

biosensor system based on carbonitride aptamer can be used for the determination of AFB_1 in real agricultural products.

4 Conclusion

In summary, we demonstrated a ECL biosensor based on g-VN that is affordable, simple and sensitive for detecting AFB_1. The use of g-CN as emitter reduces the cost of the ECL system. The amide bond between g-CN and the aptamer increases the stability of the biosensor, and specific length of aptamer was determined to selectively discern AFB_1. The composite film was revealed to be stable, specific, and regenerable. In addition, the spike-recovery test for AFB_1 in rice samples demonstrates the potential applicability of the method. Moreover, Changing the sequence and length of the aptamer could extend the range of applications of the biosensor as long as the test target could be stably present in the test liquid environment of detection experiment. However, several shortcomings require further work to circumvent such as the preparation of nanomaterials is not environmentally friendly, and the efficiency of g-CN and aptamer conjugation processes is not high enough.

Declarations

If any of the sections are not relevant to your manuscript, please include the heading and write 'Not applicable' for that section.

Funding (information that explains whether and by whom the research was supported)

This work was supported by National Key Research and Development Plan of China (2017YFC0805900).

Conflicts of interest/Competing interests (include appropriate disclosures)

The authors declare that they have no conflict of interest.

Availability of data and material (data transparency)

The data is transparent.

Code availability (software application or custom code)

Not applicable.

Authors' contributions (optional: please review the submission guidelines from the journal whether statements are mandatory)

Kejian Ding, Songmei Wu, and Yu Yu contributed to the conception of the study;

Dongyan Tian performed the experiment;

Dongyan Tian contributed significantly to analysis and manuscript preparation;

Dongyan Tian, performed the data analyses and wrote the manuscript;

Chao Lv, Haihan Zou, and Jie Wang helped perform the analysis with constructive discussions.

References

1. Rushing BR, Selim MI (2019) Aflatoxin B1: A review on metabolism, toxicity, occurrence in food, occupational exposure, and detoxification methods. Food Chem Toxicol 124:81-100. doi:10.1016/j.fct.2018.11.047
2. Wang B, Chen YF, Wu YY, Weng B, Liu YS, Lu ZS, Li CM, Yu C (2016) Aptamer induced assembly of fluorescent nitrogen-doped carbon dots on gold nanoparticles for sensitive detection of AFB(1). Biosens Bioelectron 78:23-30. doi:10.1016/j.bios.2015.11.015
3. Eivazzadeh-Keihan R, Pashazadeh P, Hejazi M, de la Guardia M, Mokhtarzadeh A (2017) Recent advances in Nanomaterial-mediated Bio and immune sensors for detection of aflatoxin in food products. Trac-Trends Anal Chem 87:112-128. doi:10.1016/j.trac.2016.12.003
4. Zhao YR, Huang JX, Ma LY, Wang FH (2017) Development and validation of a simple and fast method for simultaneous determination of aflatoxin B-1 and sterigmatocystin in grains. Food Chemistry 221:11-17. doi:10.1016/j.foodchem.2016.10.036
5. Xiong Y, Pei K, Wu YQ, Xiong YH (2017) Colorimetric ELISA based on glucose oxidase-regulated the color of acid-base indicator for sensitive detection of aflatoxin B-1 in corn samples. Food Control 78:317-323. doi:10.1016/j.foodcont.2017.03.002
6. Cao HX, Wang L, Pan CG, He YS, Liang GX (2018) Aptamer based electrochemiluminescent determination of bisphenol A by using carboxylated graphitic carbon nitride. Microchim Acta 185 (10):8. doi:10.1007/s00604-018-2997-x
7. Babamiri B, Bahari D, Salimi A (2019) Highly sensitive bioaffinity electrochemiluminescence sensors: Recent advances and future directions. Biosens Bioelectron 142:111530. doi:10.1016/j.bios.2019.111530

8. Wang YZ, Hao N, Feng QM, Shi HW, Xu JJ, Chen HY (2016) A ratiometric electrochemiluminescence detection for cancer cells using g-C3N4 nanosheets and Ag-PAMAM-luminol nanocomposites. Biosens Bioelectron 77:76-82. doi:10.1016/j.bios.2015.08.057
9. Lin X, Liu C, Wang JB, Yang S, Shi JY, Hong YZ (2019) Graphitic carbon nitride quantum dots and nitrogen-doped carbon quantum dots co-decorated with BiVO4 microspheres: A ternary heterostructure photocatalyst for water purification. Sep Purif Technol 226:117-127. doi:10.1016/j.seppur.2019.05.093
10. Lu MF, Wang WL, Zhao WL, Li QQ, Du CX, Xu JW, Fan XX, Shi HF (2019) Au-loaded porous g-C3N4 nanosheets for enhanced photocatalytic IPA degradation under visible-light irradiation. J Phys D-Appl Phys 52 (9):8. doi:10.1088/1361-6463/aaf782
11. Guo ML, Hou Q, Waterhouse GIN, Hou JY, Ai SY, Li XY (2019) A simple aptamer-based fluorescent aflatoxin B1 sensor using humic acid as quencher. Talanta 205:6. doi:10.1016/j.talanta.2019.120131
12. Jia YM, Wu F, Liu PL, Zhou GH, Yu B, Lou XD, Xia F (2019) A label-free fluorescent aptasensor for the detection of Aflatoxin B1 in food samples using AIEgens and graphene oxide. Talanta 198:71-77. doi:10.1016/j.talanta.2019.01.078
13. Ali MH, Elsherbiny ME, Emara M (2019) Updates on Aptamer Research. International Journal of Molecular Sciences 20 (10):23. doi:10.3390/ijms20102511
14. Ding JN, Liu Y, Zhang DW, Yu ML, Zhan XJ, Zhang D, Zhou P (2018) An electrochemical aptasensor based on gold@polypyrrole composites for detection of lead ions. Microchim Acta 185 (12):7. doi:10.1007/s00604-018-3068-z
15. Wang XY, Gao FX, Gong YY, Liu GT, Zhang Y, Ding CF (2019) Electrochemical aptasensor based on conductive supramolecular polymer hydrogels for thrombin detection with high selectivity. Talanta 205:6. doi:10.1016/j.talanta.2019.120140
16. Wei M, Zhang WY (2018) Ultrasensitive aptasensor with DNA tetrahedral nanostructure for Ochratoxin A detection based on hemin/G-quadruplex catalyzed polyaniline deposition. Sens Actuator B-Chem 276:1-7. doi:10.1016/j.snb.2018.08.072
17. Ge JJ, Zhao Y, Li CL, Jie GF (2019) Versatile Electrochemiluminescence and Electrochemical "On-Off" Assays of Methyltransferases and Aflatoxin B1 Based on a Novel Multifunctional DNA Nanotube. Anal Chem 91 (5):3546-3554. doi:10.1021/acs.analchem.8b05362
18. Wu L, Ding F, Yin WM, Ma J, Wang BR, Nie AX, Han HY (2017) From Electrochemistry to Electroluminescence: Development and Application in a Ratiometric Aptasensor for Aflatoxin B1. Anal Chem 89 (14):7578-7585. doi:10.1021/acs.analchem.7b01399
19. Wang C, Sun LL, Zhao Q (2019) A simple aptamer molecular beacon assay for rapid detection of aflatoxin B1. Chin Chem Lett 30 (5):1017-1020. doi:10.1016/j.cclet.2019.01.029
20. Zhang J, Yan C, Wang X (2015) Two-dimensional covalent carbon nitride nanosheets: Synthesis, functionalization, and applications. Energy & Environmental Science 8 (11):3092-3108
21. Zhang XD, Xie X, Wang H, Zhang JJ, Pan BC, Xie Y (2013) Enhanced Photoresponsive Ultrathin Graphitic-Phase C3N4 Nanosheets for Bioimaging. Journal

of the American Chemical Society 135 (1):18-21. doi:10.1021/ja308249k
22. Yu Y, Yan W, Wang XF, Li P, Gao WY, Zou HH, Wu SM, Ding KJ (2018) Surface Engineering for Extremely Enhanced Charge Separation and Photocatalytic Hydrogen Evolution on g-C3N4. Adv Mater 30 (9):8. doi:10.1002/adma.201705060
23. Mao J, Zhang LX, Wang HT, Zhang Q, Zhang W, Li PW (2018) Facile fabrication of nanosized graphitic carbon nitride sheets with efficient charge separation for mitigation of toxic pollutant. Chem Eng J 342:30-40. doi:10.1016/j.cej.2018.02.076
24. Wang BX, Zhong X, Chai YQ, Yuan R (2017) Ultrasensitive electrochemiluminescence biosensor for organophosphate pesticides detection based on carboxylated graphitic carbon nitride-poly(ethylenimine) and acetylcholinesterase. Electrochim Acta 224:194-200. doi:10.1016/j.electacta.2016.12.077
25. Niu P, Zhang LL, Liu G, Cheng HM (2012) Graphene-Like Carbon Nitride Nanosheets for Improved Photocatalytic Activities. Adv Funct Mater 22 (22):4763-4770. doi:10.1002/adfm.201200922
26. Taghdisi SM, Danesh NM, Ramezani M, Abnous K (2018) A new amplified fluorescent aptasensor based on hairpin structure of G-quadruplex oligonucleotide-Aptamer chimera and silica nanoparticles for sensitive detection of aflatoxin B-1 in the grape juice. Food Chem 268:342-346. doi:10.1016/j.foodchem.2018.06.101
27. Goud KY, Hayat A, Catanante G, Satyanarayana M, Gobi KV, Marty JL (2017) An electrochemical aptasensor based on functionalized graphene oxide assisted electrocatalytic signal amplification of methylene blue for aflatoxin B1 detection. Electrochim Acta 244:96-103. doi:10.1016/j.electacta.2017.05.089
28. Xiong XH, Li YF, Yuan W, Lu YC, Xiong X, Li Y, Chen XY, Liu YJ (2020) Screen printed bipolar electrode for sensitive electrochemiluminescence detection of aflatoxin B1 in agricultural products. Biosens Bioelectron 150:6. doi:10.1016/j.bios.2019.111873
29. Wang CQ, Qian J, An KQ, Lu XT, Huang XY (2019) A semiconductor quantum dot-based ratiometric electrochemical aptasensor for the selective and reliable determination of aflatoxin B1. Analyst 144 (16):4772-4780. doi:10.1039/c9an00825j